On quantum transport in flat-band materials

Oriekhov, D.

Chapter 8

Voltage staircase

8.1 Introduction

A single-mode weak link between superconductors supports a two-level system with a spacing that is adjustable via the superconducting phase difference [263, 264]. Because Andreev reflection is at the origin of the phase sensitivity, the levels are called Andreev levels. Although their existence was implicit in early studies of the Josephson effect [265], the characteristic dependence $\propto \sqrt{1-\tau\sin^2(\phi/2)}$ of the level spacing on the phase ϕ, with τ the transmission probability, was only identified [266] with the advent of nanostructures. The present interest in quantum information processing is driving theoretical [267, 268] and experimental [269–272] studies of Andreev levels as qubits.

To assess the coherence of the qubit one would use AC microwave radiation of the two-level system and perform a time-resolved detection of the Rabi oscillations of the wave function [273]. In this work we will show how a DC current $I_{\rm DC}$ and measurement of the time-averaged voltage $\bar{V}$ can be used to detect Rabi oscillations of an Andreev qubit: The staircase dependence of $\bar{V}$ on $I_{\rm DC}$ counts the number of Rabi oscillations per 2π increment of ϕ.

Our study is motivated by Choi, Calzona, and Trauzettel's report [55] of such a remarkable effect (dubbed "DC Shapiro steps") in a Majorana qubit — which is the building block of a topological quantum computer. As we will see, neither the unique topological properties of a Majorana qubit (its non-Abelian braiding and fusion rules) nor its specific symmetry class (class D, with broken time-reversal and spin-rotation symmetry)

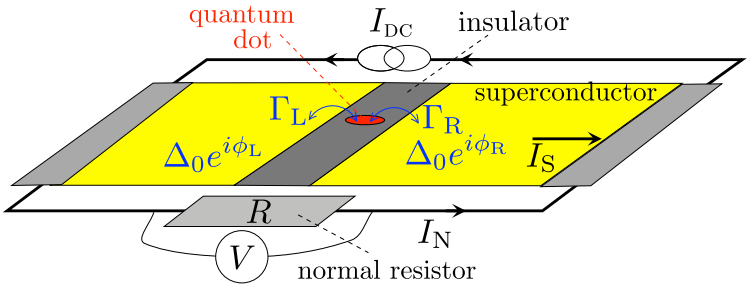

Figure 8.1. Current-biased, resistively-shunted Josephson junction, formed out of two superconductors (phases $\phi_{\rm L}$ and $\phi_{\rm R}$) separated by an insulator containing a quantum dot (tunnel rates $\Gamma_{\rm L}$ and $\Gamma_{\rm R}$ from the left and from the right). The superconducting phases become time dependent when a voltage difference V develops in response to a DC current $I_{\rm DC}$.

are needed, a similar phenomenology can be found in a non-topological Andreev qubit with preserved symmetries (class CI).

The outline of this paper is as follows. In the next section 8.2 we present the model of the weak link that we will consider: a quantum dot connecting two superconductors with a tunnel rate Γ small compared to the superconducting gap Δ_0. Such a Josephson junction has been extensively studied [274–276] in the regime where Coulomb charging and the Kondo effect govern the charge transfer [277–279]. We will assume the charging energy is small and treat the quasiparticles as noninteracting.

The dynamics of a current-biased, resistively shunted quantum-dot Josephson junction is studied in Secs. 8.3 and 8.4. The voltage staircase is shown in Fig. 8.3 and the one-to-one relationship with the number of Rabi oscillations is in Fig. 8.6. In the concluding section 7.5 we will explain why the substitution of the quantum dot by a quantum point contact will remove the voltage staircase.

8.2 Andreev level Hamiltonian

We consider the Josephson junction shown in Fig. 8.1, consisting of a quantum dot in the normal state (N) coupled via a tunnel barrier to superconductors (S) at the left and right, with pair potentials $\Delta_0 e^{i\phi_{\rm L}}$ and $\Delta_0 e^{i\phi_{\rm R}}$. We focus on the weakly coupled regime, when the tunnel rates $\Gamma_{\rm L}$ and $\Gamma_{\rm R}$ through the barrier are small compared to Δ_0.

We assume that the fully isolated quantum dot has a single electronic

energy level E_0 within an energy range $\Gamma = \Gamma_\mathrm{L} + \Gamma_\mathrm{R}$ from the Fermi energy μ. The normal-state conductance G_N is then given by the Breit-Wigner formula

$$G_\mathrm{N} = \frac{2e^2}{h}\tau_\mathrm{BW}, \quad \tau_\mathrm{BW} = \frac{\Gamma_\mathrm{L}\Gamma_\mathrm{R}}{(E_0-\mu)^2 + \frac{1}{4}\Gamma^2}. \tag{8.1}$$

Coupling of electrons and holes by Andreev reflection from the superconductor produces a pair of Andreev levels at energies $\pm E_\mathrm{A}(\phi)$, dependent on the phase difference $\phi = \phi_\mathrm{L} - \phi_\mathrm{R}$ between the left and right superconductors.

A simplifying assumption of our analysis is that the Coulomb charging energy U is small compared to Γ and can be neglected. If U is larger than Γ but still smaller than Δ_0, the main effect of the charging energy is a shift of the energy level of the dot, $E_0 \mapsto E_0 + U/2$. Provided $E_0 > 0$ the ground state remains a spin-singlet [280], and we do not expect a qualitative change in our results. If U becomes larger than Δ_0 the supercurrent is reduced by a factor Γ/Δ_0 because tunneling of a Cooper pair into the quantum dot is suppressed [277–279].

To describe the non-equilibrium dynamics of the junction we seek the effective low-energy Hamiltonian of time-dependent Andreev levels. This requires information not only on the eigenvalues but also on the eigenfunctions. In subsections 8.2.1 and 8.2.2 we summarize results from Refs. [280–283] for the time-independent situation, which we need as input for the dynamical study starting from subsection 8.2.3.

8.2.1 Andreev levels

For arbitrary ratio of Γ and Δ_0 the energies of the Andreev levels are equal to the two real solutions $\pm E_\mathrm{A}$ of the equation [281, 282]

$$\Omega(E,\phi) + \Gamma E^2\sqrt{\Delta_0^2 - E^2} = 0, \tag{8.2}$$

with

$$\begin{aligned}\Omega(E,\phi) = (\Delta_0^2 - E^2)\left[E^2 - (E_0-\mu)^2 - \tfrac{1}{4}\Gamma^2\right] \\ + \Delta_0^2\Gamma_\mathrm{L}\Gamma_\mathrm{R}\sin^2(\phi/2).\end{aligned} \tag{8.3}$$

In the weak-coupling regime $\Gamma \ll \Delta_0$, assuming also $|E_0 - \mu| \ll \Delta_0$, this reduces to

$$\begin{aligned}E_\mathrm{A} &= \Delta_\mathrm{eff}\sqrt{1 - \tau_\mathrm{BW}\sin^2(\phi/2)}, \\ \Delta_\mathrm{eff} &= \sqrt{(E_0-\mu)^2 + \tfrac{1}{4}\Gamma^2},\end{aligned} \tag{8.4}$$

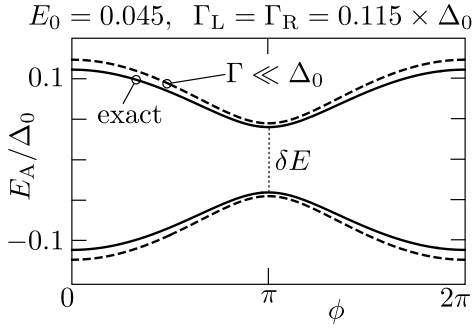

Figure 8.2. Andreev levels $\pm E_\mathrm{A}(\phi)$ according to the full expression (8.2) (solid curve) and in the weak-coupling approximation (8.4) (dashed curve, parameters $E_0 = 0.045$, $\mu = 0$, $\Gamma_\mathrm{L} = \Gamma_\mathrm{R} = 0.115$, all in units of Δ_0).

no longer dependent on Δ_0. The two Andreev levels have an avoided crossing at $\phi = \pi$, separated by an energy

$$\delta E = \sqrt{4(E_0 - \mu)^2 + (\Gamma_\mathrm{L} - \Gamma_\mathrm{R})^2}, \tag{8.5}$$

see Fig. 8.2.

The equilibrium supercurrent, at temperatures $k_\mathrm{B}T \ll \Gamma$, is given by

$$I_\mathrm{eq}(\phi) = -\frac{2e}{\hbar}\frac{dE_\mathrm{A}}{d\phi} = \frac{e\Gamma_\mathrm{L}\Gamma_\mathrm{R}\sin\phi}{2\hbar E_\mathrm{A}(\phi)}, \tag{8.6}$$

with critical current (maximal supercurrent)

$$I_\mathrm{c} = \frac{e}{\hbar}\left(\sqrt{(E_0-\mu)^2 + \tfrac{1}{4}\Gamma^2} - \sqrt{(E_0-\mu)^2 + \tfrac{1}{4}\Gamma^2 - \Gamma_\mathrm{L}\Gamma_\mathrm{R}}\right). \tag{8.7}$$

There is no contribution from the continuous spectrum in the weak-coupling regime [281].

8.2.2 Effective Hamiltonian: time-independent phase

For time-independent phases the effective low-energy Hamiltonian in the weak-coupling regime $\Gamma \ll \Delta_0$ follows from second-order perturbation theory [280, 283],

$$H = -\tfrac{1}{2}(e^{i\phi_\mathrm{L}}\Gamma_\mathrm{L} + e^{i\phi_\mathrm{R}}\Gamma_\mathrm{R})a_\uparrow^\dagger a_\downarrow^\dagger + \mathrm{H.c.} + (E_0 - \mu)(a_\uparrow^\dagger a_\uparrow + a_\downarrow^\dagger a_\downarrow). \tag{8.8}$$

Here $a_\uparrow$ and $a_\downarrow$ are the fermionic annihilation operators of a spin-up or spin-down electron in the quantum dot.

The corresponding Bogoliubov-De Gennes (BdG) Hamiltonian $\mathcal{H}$ is a 4×4 matrix contracted with the spinors $\Psi = (a_\uparrow, -a_\downarrow^\dagger, a_\downarrow, -a_\uparrow^\dagger)$ and $\Psi^\dagger$,

$$H = \tfrac{1}{2}\Psi^\dagger \cdot \mathcal{H} \cdot \Psi + E_0 - \mu. \tag{8.9}$$

It is block-diagonal, so we only need to consider one 2×2 block, given by

$$\mathcal{H} = \begin{pmatrix} E_0 - \mu & \frac{1}{2}e^{i\phi_{\rm L}}\Gamma_{\rm L} + \frac{1}{2}e^{i\phi_{\rm R}}\Gamma_{\rm R} \\ \frac{1}{2}e^{-i\phi_{\rm L}}\Gamma_{\rm L} + \frac{1}{2}e^{-i\phi_{\rm R}}\Gamma_{\rm R} & \mu - E_0 \end{pmatrix}. \tag{8.10}$$

One readily checks that the eigenvalues $\pm E_{\rm A}$ of $\mathcal{H}$ are given by Eq. (8.4).

8.2.3 Effective Hamiltonian: time-dependent phase

When the left and right superconductors are at different voltages $\pm V/2$, the superconducting phase becomes time dependent. We choose a gauge such that $\phi_{\rm L}(t) = \phi(t)/2$, $\phi_{\rm R}(t) = -\phi(t)/2$, evolving in time according to the Josephson relation

$$\dot\phi \equiv d\phi/dt = (2e/\hbar)V. \tag{8.11}$$

The voltage bias imposes an electrical potential on the quantum dot, which shifts μ by an amount $\frac{1}{2}\gamma eV$ with $\gamma = (\Gamma_{\rm L} - \Gamma_{\rm R})/\Gamma$. The time dependent BdG Hamiltonian then becomes

$$\begin{aligned}\mathcal{H}(t) &= \begin{pmatrix} E_0 - \mu - \frac{1}{4}\hbar\gamma\dot\phi(t) & \frac{1}{2}e^{i\phi(t)/2}\Gamma_{\rm L} + \frac{1}{2}e^{-i\phi(t)/2}\Gamma_{\rm R} \\ \frac{1}{2}e^{-i\phi(t)/2}\Gamma_{\rm L} + \frac{1}{2}e^{i\phi(t)/2}\Gamma_{\rm R} & \mu - E_0 + \frac{1}{4}\hbar\gamma\dot\phi(t) \end{pmatrix} \\ &= \big[E_0 - \mu - \tfrac{1}{4}\hbar\gamma\dot\phi(t)\big]\sigma_z + \tfrac{1}{2}\Gamma\big[\sigma_x\cos\tfrac{1}{2}\phi(t) - \gamma\sigma_y\sin\tfrac{1}{2}\phi(t)\big]. \end{aligned} \tag{8.12}$$

The Pauli matrices act on the electron-hole degree of freedom. The corresponding current operator is given by

$$I(t) = \frac{2e}{\hbar}\frac{\partial}{\partial\phi}\mathcal{H}(t) = -\frac{e\Gamma}{2\hbar}\big[\sigma_x\sin\tfrac{1}{2}\phi(t) + \gamma\sigma_y\cos\tfrac{1}{2}\phi(t)\big]. \tag{8.13}$$

Notice that the Hamiltonian (8.12) depends both on $\phi(t)$ and on $\dot\phi(t)$, unless $\Gamma_{\rm L} = \Gamma_{\rm R}$. It is possible to remove the $\dot\phi$-dependence by a time-dependent unitary transformation [1], but since this does not simplify our subsequent calculations we will keep the form (8.12).

[1] The time-dependent unitary transformation $\Psi \mapsto U^\dagger\Psi$, $\mathcal{H} \mapsto U^\dagger\mathcal{H}U - i\hbar U^\dagger dU/dt$ with $U(t) = e^{i\sigma_z\gamma\phi(t)/4}$ removes the $\dot\phi$-term from the Hamiltonian (8.12). The γ-parameter then appears in the superconducting phases, $\phi_{\rm L} = \frac{1}{2}(1-\gamma)\phi$, $\phi_{\rm R} = -\frac{1}{2}(1+\gamma)\phi$.

8.3 Voltage staircase

As shown in Fig. 8.1, a time-independent current bias $I_{\rm DC}$ is driven partially through the Josephson junction, as a supercurrent $I_{\rm S}(t)$, and partially through a parallel resistor R as a normal current $I_{\rm N}(t) = V(t)/R$. Substitution of the Josephson relation (8.11) gives the differential equation

$$d\phi(t)/dt = (2eR/\hbar)[I_{\rm DC} - I_{\rm S}(t)]. \tag{8.14}$$

Here we neglect the junction capacitance (overdamped regime of a resistively shunted Josephson junction) [284]. We work in the low-temperature regime, $k_{\rm B}T \ll \Delta_0$, so that we may ignore thermal fluctuations of the phase due to the voltage noise over the external resistance [285].

The supercurrent is obtained from the expectation value

$$I_{\rm S}(t) = \langle\Psi(t)|I(t)|\Psi(t)\rangle, \tag{8.15}$$

where the current operator is given by Eq. (8.13) and the wave function evolves according to the Schrödinger equation

$$i\hbar\frac{d}{dt}|\Psi(t)\rangle = \mathcal{H}(t)|\Psi(t)\rangle. \tag{8.16}$$

As initial condition we take $\phi(0) = 0$ and $|\Psi(0)\rangle$ the eigenstate of the Andreev level at $-E_{\rm A}$ for $\phi = 0$. The DC current $I_{\rm DC}$ is increased slowly from zero to some maximal value and then slowly decreased back to zero. The I–V characteristic is obtained by averaging $V(t)$ over a moving time window in which $I_{\rm DC}$ is approximately constant.
[2]

Results of this numerical integration are shown in Fig. 8.3. We observe a staircase dependence of $\bar{V}$ on $I_{\rm DC}$. The nonzero voltage appears at the critical current (8.7) for the up-sweep and disappears at a slightly lower current for the down sweep. (A similar difference between switching current and retrapping current was found for the Majorana qubit [286].) The voltage steps at $I_{\rm DC} > I_c$ also show hysteresis: the voltage jump up happens at larger DC current than the voltage jump down. (This hysteresis also appears in the Majorana qubit, see App. 8.6.)

[2]The parameters $E_0, \Gamma_{\rm L}, \Gamma_{\rm R}$ used in Fig. 8.3 are listed in each panel; additional parameters: $\mu = 0$ in both panels, $R = 0.20$ and $0.25\,\hbar/e^2$ in panels a) and b), respectively. The voltage $\bar{V}$ is averaged over a time window δt such that $\delta t \times dI_{\rm DC}/dt = 6.3 \cdot 10^{-4}\, e\Delta_0/\hbar$. To check that we are sweeping slowly enough, we reduced $dI_{\rm DC}/dt$ by a factor of two and found little difference.

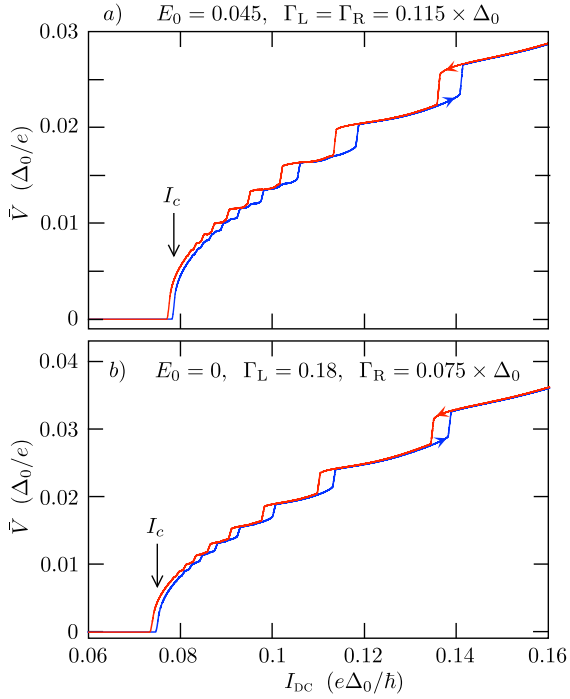

Figure 8.3. Current-voltage characteristic of the quantum-dot Josephson junction, for two different parameter sets2. The blue curve is for increasing DC current, the red curve for decreasing current. The Andreev levels in Fig. 8.2 correspond to the parameters in panel a). The critical current (8.7) is indicated by the black arrow.

8.4 Andreev qubit dynamics

The voltage staircase of Fig. 8.3 is a signature of Rabi oscillations of the Andreev qubit formed by the two Andreev levels in the Josephson junction, in much the same way that the voltage steps of Ref. [55] were driven by Rabi oscillations of a Majorana qubit. Let us investigate the Andreev qubit dynamics.

8.4.1 Adiabatic evolution

In the adiabatic regime of a slow driving, $\hbar\dot{\phi} \ll \delta E$, transitions between the Andreev levels can be neglected and the phase evolves in time as an

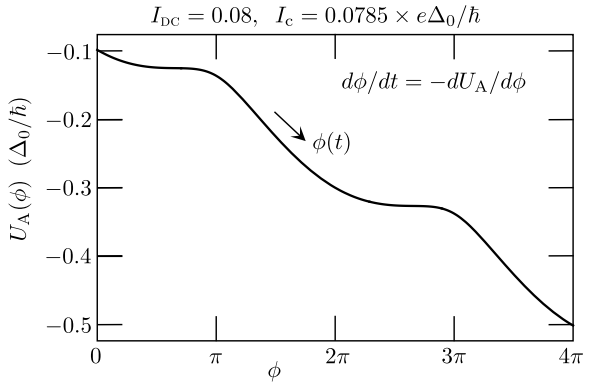

Figure 8.4. Washboard potential (8.18) that governs the time dependence of the superconducting phase in the adiabatic limit. The curve is plotted for the junction parameters of Figs. 8.2 and 8.3a, at a value of $I_{\rm DC}$ slightly above the critical current $I_{\rm c}$.

overdamped classical particle,

$$\dot{\phi} + dU_{\rm A}/d\phi = 0, \tag{8.17}$$

moving in the "washboard potential" [284]

$$U_{\rm A}(\phi) = -(2eR/\hbar)\big[\phi I_{\rm DC} + (2e/\hbar)E_{\rm A}(\phi)\big], \tag{8.18}$$

plotted in Fig. 8.4.

The time dependence of the phase resulting from integration of Eq. (8.17) is shown in panel a) of Fig. 8.5. Panel b) tracks the adiabatic dynamics of the Andreev qubit, by plotting the Bloch sphere coordinates $\boldsymbol{R} = (X, Y, Z)$, with $R_\alpha(t) = \langle\Psi(t)|\sigma_\alpha|\Psi(t)\rangle$. The qubit dynamics is 4π-periodic in ϕ, because the Hamiltonian (8.12) is 4π-periodic: When ϕ is increased by 2π one has $\mathcal{H} \mapsto \sigma_z\mathcal{H}\sigma_z$, so on the Bloch sphere the qubit is rotated by π around the z-axis ($X \mapsto -X$, $Y \mapsto -Y$). The full spectrum is a 2π-periodic function of ϕ, in particular the Josephson current (8.6) is 2π-periodic — this nontopological Josephson junction does not exhibit the 4π-periodic Josephson effect that is the hallmark of a topological superconductor.

8.4.2 Pulsed Rabi oscillations

Panels c) and d) of Fig. 8.5 show the full non-adiabatic dynamics, obtained by integration of Eq. (8.16) for the same parameter set as in panels a) and

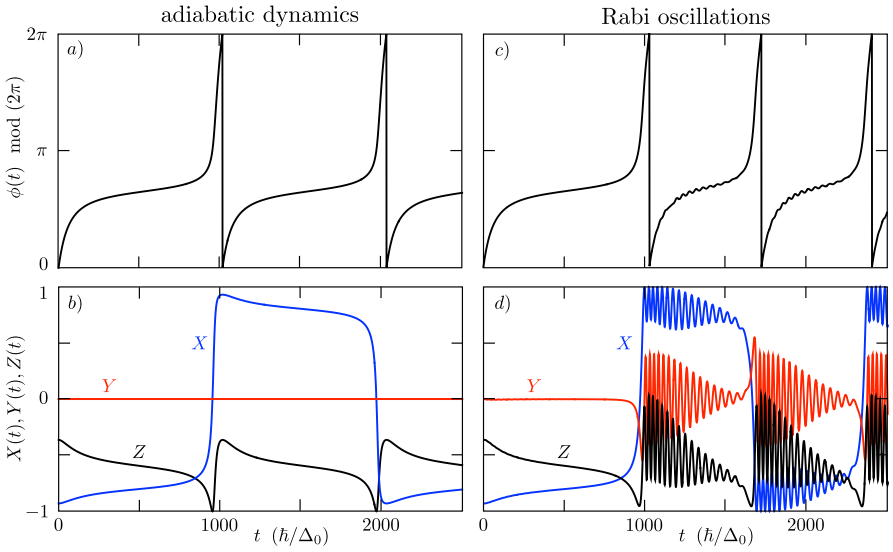

Figure 8.5. Time dependence of the superconducting phase (top row) and of the Bloch sphere coordinates of the Andreev qubit (bottom row), in the adiabatic limit (left column) and in the non-adiabatic regime in which transitions between the Andreev levels produce Rabi oscillations of the qubit (right column). The junction parameters are those of Fig. 8.3a, at $I_{\rm DC} = 0.08\, e\Delta_0/\hbar$. The wave function was initialized as an eigenstate of the lowest Andreev level $-E_{\rm A}(0)$ at $t = 0$.

b). Transitions between the Andreev levels produce pronounced Rabi oscillations of the qubit, also visible as small oscillations in $\phi(t)$.

Because the supercurrent carried by the two Andreev levels $\pm E_{\rm A}$ has the opposite sign, the inter-level transitions reduce $I_{\rm S}$, thereby increasing $I_{\rm N} = I_{\rm DC} - I_{\rm S}$ and hence $\bar{V}$. This is evident from Fig. 8.5c, which shows that the first 2π increment of ϕ, without interlevel transitions, takes a time $\delta t \approx 1000\,\hbar/\Delta_0$, while the second 2π increment, with Rabi oscillations, only takes a time $\delta t = 700$. The average voltage $\bar{V} \simeq 2\pi/\delta t$ is therefore increased by a factor 10/7 because of the interlevel transitions.

The Rabi oscillations are pulsed: they appear abruptly when ϕ crosses $(2n-1)\pi$ and increases rapidly to $2n\pi$, which is the steepest part of the washboard potential (see Fig. 8.4).

To estimate the Rabi frequency we substitute

$$\Psi(t) = \left(u(t)e^{i\phi(t)/4}, v(t)e^{-i\phi(t)/4}\right)$$

in the Schrödinger equation (8.16) and make the rotating wave approximation, discarding rapidly oscillating terms $\propto e^{i\phi(t)}$:

$$\begin{aligned} i\hbar\dot{u}(t) &= [E_0 - \mu + \tfrac{1}{2}eV(t)]u(t) + \tfrac{1}{4}\Gamma v(t), \\ i\hbar\dot{v}(t) &= -[E_0 - \mu + \tfrac{1}{2}eV(t)]v(t) + \tfrac{1}{4}\Gamma u(t). \end{aligned} \tag{8.19}$$

(We have set $\Gamma_{\rm L} = \Gamma_{\rm R}$ for simplicity.) If we further neglect the slow time dependence of the voltage, we obtain oscillations $\propto \sin^2 \omega_{\rm R} t$ of the Bloch vector components X, Y, Z with Rabi frequency

$$\hbar\omega_{\rm R} = \sqrt{(E_0 - \mu + \tfrac{1}{2}eV)^2 + (\Gamma/4)^2}. \tag{8.20}$$

The oscillations in Fig. 8.5d near $t = 1000\times\hbar/\Delta_0$ have a period of $35\,\hbar/\Delta_0$, while $T_{\rm R} = \pi/\omega_{\rm R} = 40\,\hbar/\Delta_0$ if we set $V = RI_{\rm DC}$, in reasonable agreement.

8.4.3 Voltage steps count Rabi oscillations

The key discovery of Ref. [55] is that steps in the time-averaged voltage track the change in the number of Rabi oscillations of the Majorana qubit per 2π increment of the superconducting phase. Fig. 8.6 shows the same correspondence for the Andreev qubit.

If we estimate the duration δt of a 2π phase increment by the product of the number N of Rabi oscillations and the Rabi period $T_{\rm R}$, we obtain the estimate $(2e/\hbar)\bar{V} = 2\pi/\delta t \simeq 2\omega_{\rm R}/N$. A stepwise decrease of N with increasing $I_{\rm DC}$ would then produce a stepwise increase of $\bar{V}$. This argument is suggestive, but does not explain the sharpness of the steps. We have no quantitative analytical derivation for why the steps are as sharp as they appear in the numerics.

8.5 Discussion

Two lessons learned from this study are: 1) Rabi oscillations of an Andreev qubit can be counted "one-by-one" without either requiring time-resolved detection or AC driving; 2) The voltage staircase phenomenology of Ref. [55] does not need a topological Majorana qubit — it exists in a conventional Andreev qubit.

We worked in the weak-coupling regime $\Gamma \ll \Delta_0$ because it simplifies the calculations, but also for a physics reason: The voltage staircase is suppressed when Γ becomes larger than Δ_0, due to a well-known decoherence

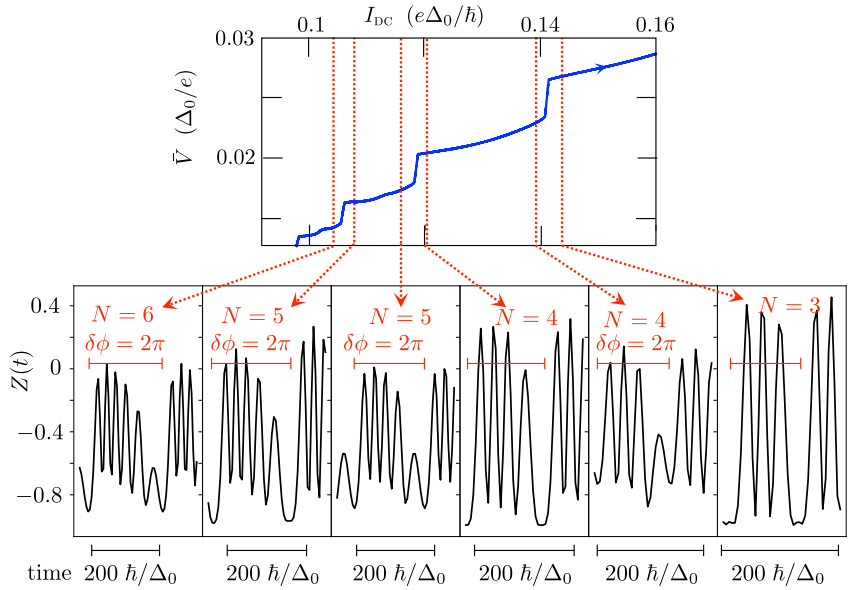

Figure 8.6. Top panel: portion of the I–V characteristic from Fig. 8.3a, with red dotted lines into the the bottom panels to show how the voltage steps line up with the change in the number N of Rabi oscillations of the qubit in a 2π phase increment $\delta\phi$.

mechanism [285, 287]: Equilibration of the Andreev levels $\pm E_{\rm A}(\phi)$ with the continuous spectrum at $|E| > \Delta_0$ when ϕ crosses an integer multiple of 2π. Let us discuss this in a bit more detail.

For $\Gamma \gg \Delta_0$ the Andreev levels are given by

$$E_{\rm A} = \Delta_0 \sqrt{1 - \tau_{\rm BW} \sin^2(\phi/2)}, \tag{8.21}$$

according to Eq. (8.2), with $\tau_{\rm BW}$ the Breit-Wigner transmission probability (8.1). The difference with the weak-coupling result (8.4) is that the reduced gap $\Delta_{\rm eff}$ has been replaced by the true gap Δ_0. This means the Andreev level merges with the superconducting continuum whenever $\phi = 0$ modulo 2π. As the phase evolves in time in response to the current bias, each 2π phase increment will restart from an equilibrium distribution.

Now if we examine Fig. 8.5, panels c) and d), we see that the Rabi oscillations are pulsed by the rapid increase of the phase in the $(\pi, 2\pi)$ interval, and only fully develop in the $(2\pi, 3\pi)$ interval. Equilibration at

$\phi = 2\pi$ will restart the cycle from $t = 0$, suppressing the Rabi oscillations and hence the voltage staircase.

For the same reason a superconducting quantum point contact will not show the voltage staircase: its Andreev levels also reconnect with the superconducting continuum at $\phi = 0$ modulo 2π.

This argument points to one difference in the Majorana versus Andreev phenomenology of the voltage staircase: A topological Josephson junction needs to be magnetic in order to prevent the equilibration of the Majorana modes with the continuum at $\phi = 0$ modulo 2π [246]. In a non-topological quantum-dot Josephson junction this can achieved without breaking time-reversal symmetry.

As a topic for further research, it would be worthwhile to see if the voltage staircase can be used to count the number of Rabi oscillations over multiple 2π phase increments, since that would provide additional information on the coherence time of the qubit. This could involve the constructive interference of Landau-Zener transitions at $\phi = \pi, 3\pi, \ldots$ [288].

8.6 Appendix: Hysteresis of the voltage staircase for the Majorana qubit

The voltage staircase of the Andreev qubit is hysteretic, the steps appear at higher current for the up-sweep than for the down-sweep. No hysteresis was reported in Ref. [55], here we show that it is present for the Majorana qubit as well.

Instead of Eqs. (8.12) and (8.13) one has for the Majorana qubit the time dependent Hamiltonian

$$\mathcal{H}(t) = E_x\sigma_x + E_z\sigma_z \cos\tfrac{1}{2}\phi(t), \tag{8.22}$$

and current operator

$$I(t) = \frac{2e}{\hbar}\frac{\partial}{\partial\phi}\mathcal{H}(t) = -\frac{eE_z}{\hbar}\sigma_z \sin\tfrac{1}{2}\phi(t). \tag{8.23}$$

The Pauli matrices act on the fermion parity of two pairs of Majorana zero-modes, such that σ_x flips the even–even parity state into the odd–odd parity state, while σ_z changes the sign of the odd–odd parity state. While the physical origin of the Majorana coupling terms is different from the

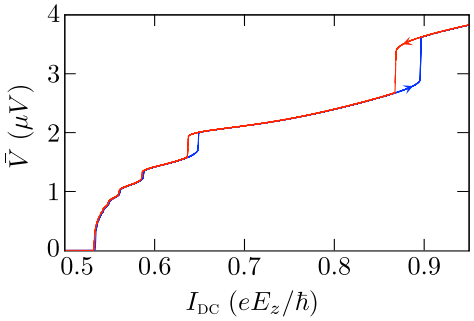

Figure 8.7. Hysteretic voltage staircase of the Majorana Josephson junction, for the parameters of Ref. [55], Fig. 3. The blue curve is for increasing DC current, the red curve for decreasing current. (The voltage $\bar{V}$ is averaged over a time window δt such that $\delta t \times dI_{\rm DC}/dt = 10^{-3}\, eE_z/\hbar$.)

Andreev qubit, mathematically the Hamiltonian (8.22) is equivalent to Eq. (8.12) in the symmetric case $\Gamma_{\rm L} = \Gamma_{\rm R}$. (Switch $\sigma_x \leftrightarrow \sigma_z$ by a unitary transformation and replace $E_x \mapsto E_0 - \mu$ and $E_z \mapsto \Gamma/2$.)

In Fig. 8.7 we show the hysteretic voltage staircase, for the same parameters $E_z = 5\,\mu$eV, $E_x/E_z = 0.67$, $R = 0.827\,\hbar/e^2$ as in Ref. [55].